Optimized Radar Signal Processing for a Low-cost, Solid-State Airborne Radar

Yan Zhang[1], Zhengzheng Li[1], Boonleng Cheong[1], Jingxiao Cai[1], Nepal Ramesh[1], Hernan Suarez[1], William Blake[2], Joel Andrews[2] and Teoh Yong[2]
[1]Intelligent Aerospace Radar Team, Advanced Radar Research Center, Norman, OK 73072
[2] Garmin Aviation Weather Radar Group, Olathe, KS 66062

1. INTRODUCTION

Hazard sense and avoid (H-SAA) is an emerging new type of radar sensing mission mainly for unmanned aerial system (UAS) integration and aviation safety. This work studies the fundamental requirements and challenges of H-SAA radars, and uses both simulation and Garmin's GWX-70 radars testbeds to investigate how the H-SAA missions could be accomplished by enhancing the current low-cost solid-state airborne weather systems originally designed for commercial airplanes. A two-dimensional signal processing solution is proposed as the key, and the practical aspects of implementing this solution are discussed.

2. BASICS OF H-SAA RADAR SENSING

The missions of H-SAA include collision avoidance, self-separation and aviation hazard monitoring (ASTM Standard F2411, 2007). In conjunction with other radar sensors, SAA radar is mainly for unmanned aerial system to support the safety of the platform and situation awareness under all-weather condition. For non-cooperative target collision avoidance, the operating range is relative short (i.e., less than 6 nautical miles), and the resolution needs to be very high to discriminate and precisely locate multiple moving targets for precise maneuver control, and it should be comparable to transponder based collision avoidance system such as TCAS and ADS-B. The main interested targets are aircrafts that do not have functional transponder systems, while since 2007, DoD/NASA have started investigating the incorporation of adverse weather as part of the hazards. Meteorological aviation hazards, such as convective storms, snow, hail, turbulence, and wind shear and wake vortices have been severe issues related to airspace capacities, transportation delays, instrumentation meteorological conditions (IMCs), and environmental impact on SAA sensors (Angelov, 2012, Griffith, 2011).

Table 1 compares the two fundamental types of SAA radar operations – Ground Based (GB) and Airborne (AB) SAAs. In this study, we focus on AB-SAA functions based on a low-cost, solid-state weather radar produced from Garmin International, Inc. The specifications of this radar are listed in (Garmin 2013).

	GBSAA	ABSAA
Mission	Monitoring non-cooperative aircraft and weather from ground	Monitoring non-cooperative aircraft and weather onboard
Sensors	Ground based multi-functional radar or mobile radars	Airborne multi-function radars
Example radar systems	ASR (being tested), MPAR, and mobile X-band radars (MATS, SAVDS)	Ka band AI-130 Radar. Northrop Grumman BAMS RQ-4N, ITT Exelis- MQ-4C, NASA-ERAST-OASys
Advantages	Can upgrade from existing ATC systems, support small UAs, do not need to modify UAs	Localized, fast update and real-time Non-interrupted through mission
Disadvantages	Volume coverage is limited Update rate is slow Affect by ground clutters and many clutters near ground	Need UA payloads Limited field of regard Technology still being developed

Table 1: Ground based and Airborne SAA

There are important reasons that the GWX-70 radar (Garmin, 2013) is selected to be used in this investigation. It is an X-band solid-state radar product used widely in existing general aviation and commercial aircrafts. It has the desired SWaP (Space, Weight and Power consumption) as it only uses 20 by 16 cm size profile, less than 10 lbs in weight, and less than 50 watt total power consumption. The cost of this system is much lower than other similar products.

The main focus of this work is the feasibility of improving the current solid-state radar product such as GWX-70 to achieve the H-SAA missions. The fundamental challenge of such application originates from the pulsed solid-state implementation. First, the longer transmit pulse for solid-state radar enlarges the "blind-range", which is the near range in proportional to the pulse length, so the important zones for collision avoidance can be overwhelmed by the direct-coupled transmit pulse itself. Second, the range sidelobes due to pulse compression waveforms can cause weather targets "masked" by stronger targets, or biased estimation of reflectivities/Doppler velocities. Third, the aperture limitation of the existing radar products poses a hard limitation of angular resolution, which not only restricts

*Corresponding author: Yan Zhang, School of Electrical and Computer Engineering, University of Oklahoma, Norman OK 73072, Email: rockee@ou.edu

target discrimination capability but also destroys the quality of further processing such as polarimetric feature extractions. These issues must be addressed before a reliable SAA mission can be performed.

3. PROBLEM FORULATION AND SIGNAL PROCESSING (SP) SOLUTIONS

3.1 Problem Analysis

The ultimate solutions of these issues mentioned in last section are infinite physical aperture size and infinite transmit signal bandwidth. For low SWaP airborne radar, these are not feasible. Synthetic Aperture (SA) is a way to improve angular/cross-range resolution, but for fast moving airborne targets and distributed targets, SA does not have the real-time capability for imaging before the signals are decorrelated. For enhancing range resolution, some of the existing SAA radar prototypes use FMCW waveforms to achieve larger bandwidth and good Doppler sensing. But as a continuous wave waveform, it has intrinsic disadvantages over pulsed waveforms, such as TR coupling.

Instead of trying to improve physical aperture design and hardware components, this work develops a signal-processing based solution framework based on optimal estimation theory. Figure 1 provides an analysis of the estimation problem with a conceptual PPI scan.

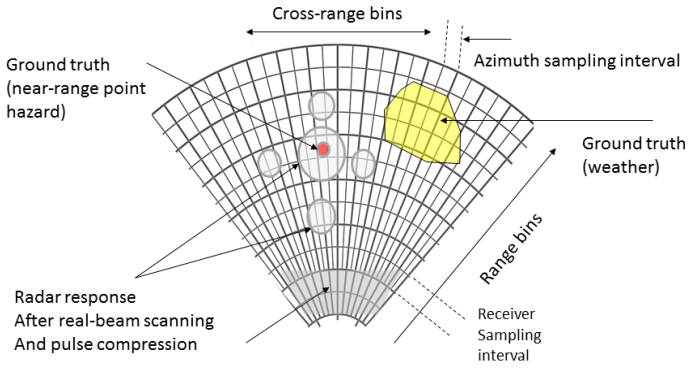

Figure 1: Problem analysis with normal forward-looking PPI scan using solid-state radars

The yellow and red colors in Figure 1 represent ground truths of distributed and hard targets. These ground truths can be expressed as target impulse responses (the back scattering voltage outputs from receiver when the targets are excited by impulses). For point targets, the impulse response is

$$h(t,\tau,\varphi) = \eta(\tau,\varphi)\,\delta(t) \qquad (1)$$

Which is Delta-function modulated by a factor in the particular cell at range/delay τ and φ. For distributed targets, the impulse response is a continuous function of space and time.

As shown in Figure 1, normal PPI scan outputs with matched filtering result in distortions in the target responses from the ground truths, for point targets, the responses are similar to the "point-spreading function" usually studied in SAR imaging. One of the challenges is to "retrieve" ground truth from these responses. It is noted that the range bin intervals (receiver sampling interval) can be shorter that the range resolution units determined by the waveform bandwidth, the cross-range bin intervals (antenna scanning steps) can be smaller than the antenna beamwidth.

3.2 SP Solutions

The main advantage of SP solutions is the "software-defined", super-resolution performance without modifying the existing sensor front-end hardware. Computational load is added as a cost, but the onboard computing power is growing very fast, and the DSPs and FPGAs are becoming cheaper, faster, and lower-power. There are two different paths of SP solutions:

A. Consider a global 2D deconvolution problem: The received radar signals can be modeled as

$$y(t,\tau,\varphi) = s(t) * h(t,\tau,\varphi) * A(\varphi) \qquad (2)$$

Essentially, this is a 2D convolution with transmit waveform and antenna pattern (only azimuth pattern is considered here). Once (2) is digitized and transformed to matrix formations, there are a lot deconvolution algorithms can be used, such as Least Square Estimation (LSE), segmented LSE, Recursive Least Squares (RLS) and its improvements, Conjugate Gradient (CG), etc. There are tremendous studies of these algorithms in the literatures and they can also be modified to work with matched filter outputs.

Although algorithms developed along this path have the optimal performance in simulations, the problems of them when implemented in real radars are significant. First, these algorithms are different ways to solve a global linear equation system, thus they are very sensitive to any small errors in waveform samples, data alignments and numerical disturbance. Results from real radar data often show instabilities.

B. Consider a localized 2D estimation problem: Instead of pursing a global solution for estimation, we can focus on each individual $h(t,\tau,\varphi)$ and try to use the received signals surrounding this particular cell to estimate the ground truth in this cell. Since the impact of the "point spreading function" usually significant only for limited cells locally, this approach is reasonable and efficient. Specifically, the minimum mean-squared error (MMSE) estimation can be developed to approach a solution that satisfies

$$\min E\left\{\left|w(\tau,\varphi) * y(t,\tau,\varphi) - h(t,\tau,\varphi)\right|^2\right\} \qquad (3)$$

In (3), $w(\tau,\varphi)$ is the MMSE filter coefficient and it spans across a limited range of

$$\tau_1 \le \tau \le \tau_2, \varphi_1 \le \varphi \le \varphi_2 \quad (4)$$

(3) can also be converted to the matrix format and a recursive procedure can be derived, which leads to the adaptive pulse compression (APC) algorithms. Traditional APCs uses y, s, A as its inputs. However, many operating radars already implemented pulse compression and the easily available inputs should be

$$\overline{y}(\tau, \varphi) = s^*(t) * y(t, \tau, \varphi) \quad (5)$$

The recursive MMSE algorithm based on $\overline{y}(\tau, \varphi)$ as inputs is called MF-RMMSE, and it is developed by OU-IART through NASA-sponsored projects. MMSE type of processing is adopted in this project for implementations. Table 2 provides a comparison of computational load and basic features of the different processing algorithms.

Algorithm (1D)	**Computational complexity**	**Features**
Matched Filter (MF)	O(N) Per range/angular cell N as the length of waveform	Simplest and standard
LS –type solution		
Normal LSE	O(L^2) per gate, L is total # of range gates	Large computation load and sensitive to errors
Segmented LSE	O(M(L/M)^2) per gate, M is # of segments	Loss of information due to segmentation (can be improved using random segmentation)
RLS	O(N^3) Per range/angular cell	Reiterative LS
Improved RLS	O(N^2) Per range/angular cell	Reduced computation of RLS
MF-RLS	O(N^2) Per range/angular cell	RLS use MF output as input
conjugate gradient (CG)	O($L^{1.5}$), L is total # of range gates	Another method to reduce computational load of LS
MMSE-type estimation		
RMMSE (APC)	O(N^3) Per range/angular cell	Reiterative MMSE with no prior knowledge of GT
MF-RMMSE	O(KN+K^3) per gate, K is filter length	RMMSE use MF output as input, usually K<<N

Table 2: Comparison of different SP algorithm solutions

For 2D estimation solutions, the next key question is if we should develop a 2D APC processing or performing sequential 1D APCs on range and azimuth. This problem is analyzed in detail in (Shang, 2012), here only the key conclusions are summarized: (1) In term of AMSE (averaged mean-squared error) performance, results from doing 2D RMMSE and sequential 1D processing do not have significant differences, except that 2D processing has a little better SNRs for weak targets. (2) In term of computational load, the computational load of 1D sequential processing grows much faster than that of 2D processing with respect to larger numbers of resolution cells. Therefore, for low-SNR and large surveillance scene, 2D RMMSE has clear advantages.

The current experiments with GWX-70 radar have been using 1D sequential processing for these reasons: (1) SAA scenarios intend to use short pulse-length, simple waveforms for short-range targets, and the current studies have been doing off-line processing, so the computational load is not an issue. (2) SNR for these scenarios are presumably high (> 15 dB), (3) It is easier to study and evaluate the impact of range and azimuth processing separately.

4. SIMULATION SCENARIOS

A series of simulations/emulations have been used to study the performance of various SP solutions for typical H-SAA scenarios, such as shown in Figure 2. Through a typical range or cross-range profile, we have direct coupling return from transmitter, near range hard targets, weather targets with Doppler, and multiple point targets with larger Doppler shifts.

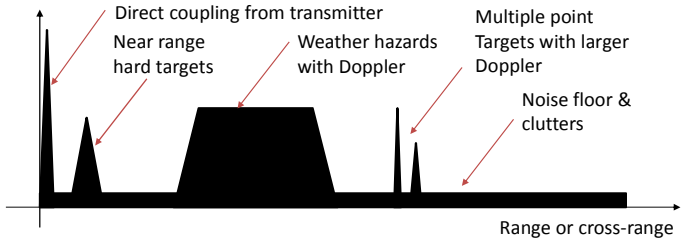

Figure 2: Simulation scenarios for typical ABSAA radar operation

Example simulation profile using 64-bit LPK3 waveform is shown in Figure 3, based on a scenario outlined from Figure 2. The phase values for the profile are also added and estimated. MF-RMMSE has been using a filter length of 11 and thus has much lower computation time than RMMSE.

All the algorithms simulated here behave well and compared to the MF outputs, the sidelobes are greatly reduced and a weather target originally masked by main sidelobe of direct coupling is now revealed.

It is important to observe the performance of phase estimation of ground truth for single-pulse range profile, as it is closely related to the Doppler estimation accuracies. In Figure 3(b), we can see MF has poor performance on estimating phase when the sidelobe interference presents, while other algorithms are able to maintain accurate estimations.

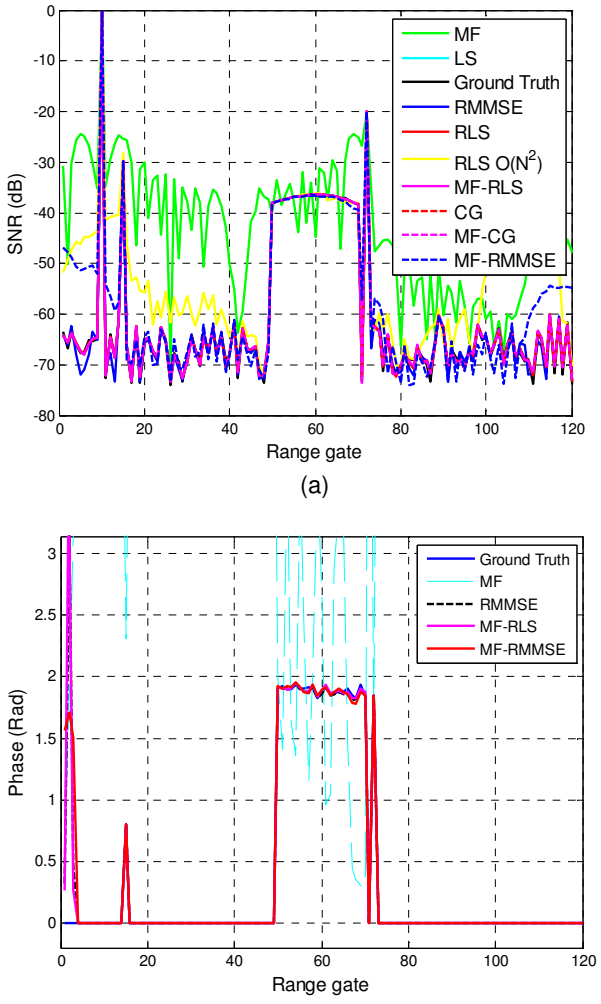

Figure 3: Sample range processing simulations using 64-bit P3-phased coded waveform, (a) power estimation, (b) phase estimation.

Another simulation example used a modified LFM waveform for testing. This is one of the waveforms being used in GWX radar. The pulse length is about 6 μs and modulation bandwidth is 2 MHz. With similar ground truth profile as in Figure 3, the comparison results are shown again in Figure 4. Although there are significant changes of MF sidelobe structures, all the APC algorithms still perform well for both power and phased estimations. It is noted that MF does better for phase modulation compared to Figure 3, as a result of improved waveform design.

In actual implementations, we usually need to down-sample the waveform and received profiles before the adaptive processing is applied. For example, if a 10 MHz digital receiver sampling rate is used and waveform analog bandwidth is 5 MHz, we may do down-sapling by factor of 2 to match them. The main reason for doing this to maintain a good SNR (comparable to MF) while remove sidelobe interferences, mainly for distributed targets. Further simulation has shown that "matching down-sampling" can still result in better resolution than MF when APCs are applied. On the other hand, cautions are needed when particular waveforms are used, especially for waveforms whose characteristics change with sampling rate, such as Nonlinear LFMs.

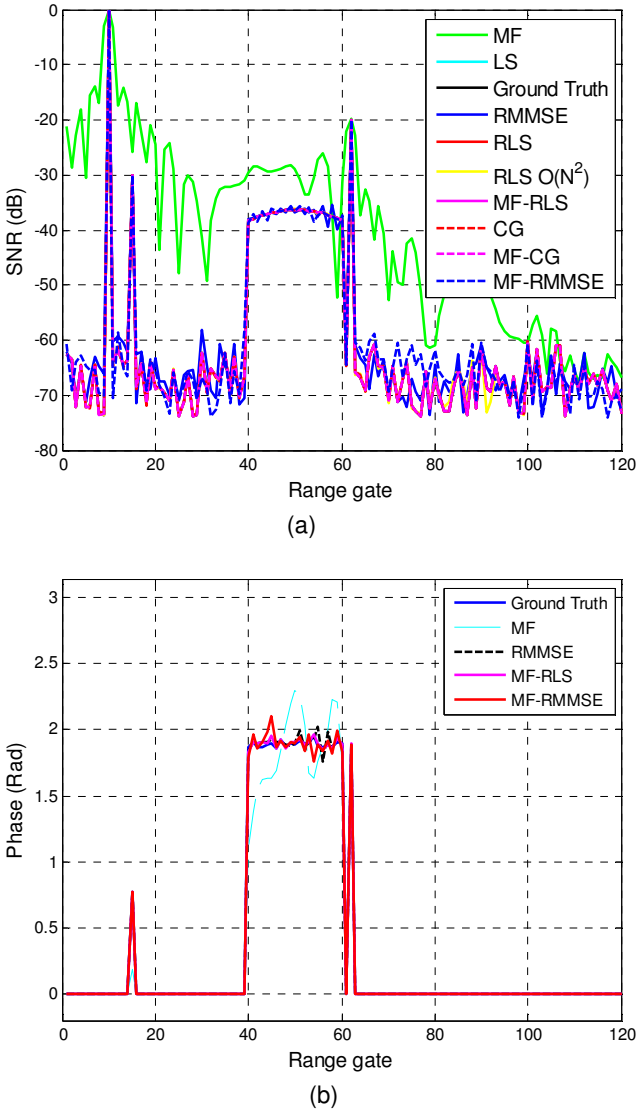

Figure 4: Sample range processing simulations using a modified LFM waveform used in GWX radar, (a) power estimation, (b) phase estimation.

From simulation and initial implementations, we conclude that algorithms based on localized 2D processing (APC, RMMSE, MF-RMMSE) are more flexible and numerically stable against ground truth variations/waveform template errors. APCs are used for the following processing examples. One important aspect is the selection of filter lengths, learning step size and number of iterations, which directly impacts the computational complexity and speed.

This is a complicated theoretical issue and will be further studied. However, extensive simulation and data analysis show that a small number of filter length (~5) and iterations (less than 5) are sufficient to achieve good estimation performance for MF-RMMSE, while it relates to the waveform and nature of targets. For discrete point targets, learning step size can be larger so the sidelobes are quickly removed and filter length can be very small (such as 3-5). For distributed weather targets, learning factor should be really small (α~1), in the meantime more iterations and longer filter length may be needed. Using different waveforms also leads to some differences in performance.

One example of range processing with simple discrete target is shown in Figure 5. The target is a water tower (steel cylinder) with 30 m height and 10 m diameter, located at near distance from GWX radar. Figure 5(a) shows the image of this target, and 5(b) shows processing results.

(a)

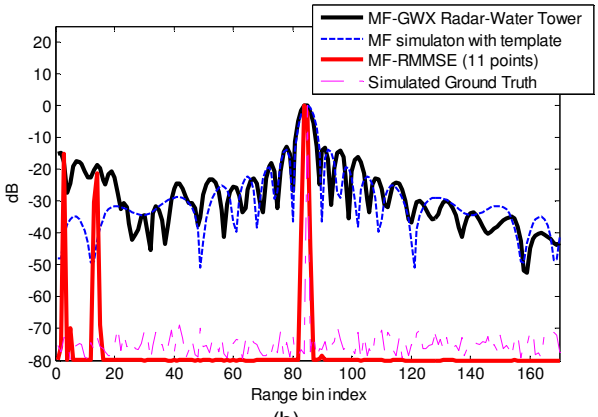

(b)

Figure 5: Range processing for single point target using MF-RMMSE, (a) target photo, (b) processing result. Number of iteration is 4.

In the results of Figure 5(b), "simulated ground truth" is simply a delta function at the location of target convoluting with the transmit waveform. The simulated matched filter output (blue) is applying the waveform template to the simulated ground truth, which is identical to the measured matched filter output (black). Applying 11-point MF-RMMSE with a large learning step size (α=3) results in extremely low range sidelobe response (red) of this point target (below the -70 dB noise floor). Also note that there are two more distinct near-range ground clutter targets shown up in the MF-RMMSE results. Comparing to 64-point waveform template, 11-point filter is quite efficient and can be further reduced.

For traditional RMMSE, on the other hand, the required filter length is always equal to the length of waveform (64-point is needed for this example). Reducing dimension is possible with loss of information and performance, and the performance is very sensitive to waveform template change (even by reducing 1-2 points). There is an exceptional scenario, however, when the waveform template itself has a clear amplitude pulse shape (either pulsed waveform, or deeply amplitude modulated), the RMMSE filter length maybe reduced since the "contribution" from waveforms samples toward pulse edges are less and less significant. This phenomenon is the basis for using shorter MMSE filter for azimuth processing.

5. PRILIMINARY IMPELEMNTATION ON GWX-70 RADAR

Based on the studies above, a preliminary procedure of APC implementation on GWX-70 radar for H-SAA application is developed and outlined in Figure 6. From radar hardware, the already pulse-compressed I/Q data for each scan is sent to the processor to form a "4D data cube", in which IQ pulses are arranged for each scan, each range, azimuth and pulse for the dwell. In the next step, the IQ data are re-sampled to match the antenna scanning sampling step and compressed pulse width. Then the data enters the most important stage of 2D processing.

Within the 2D processing module, the waveform and antenna pattern templates are also re-sampled and stored beforehand. Range processing using MF-RMMSE is applied first to each range profile of a scan, with a fixed filter length (5-point or 3-point). The range processing results for each scan and each pulse are saved for further processing. The cross-range/azimuth RMMSE processing is then applied on the results of range processing, with a filter length covering the 3dB beamwidth (for example, a 5-point filter is used to cover the 5-degree beamwidth). In the last step, the 2D processing results for all the available pulses are averaged to obtain the final 2D outputs.

Even the learning step size is set to almost one and filter lengths are short, it is found that 3 iterations for both range and cross-range processing are able to achieve converged results. The computational load is still very significant though for sequential processing. When 7 parallel cores of an AMD FX-8150 CPU is used, complete 2D processing of a 2D scene consisting by 721 range bins and 121 azimuth bins takes approximately 10 minutes. Currently a Graphic

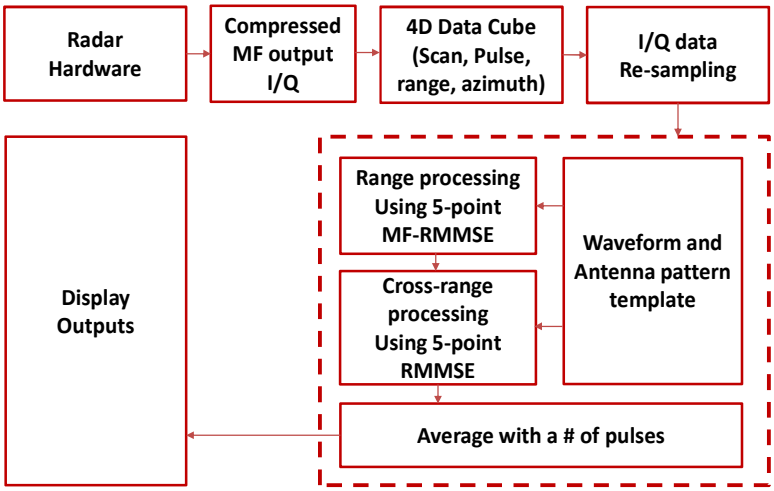

Figure 6: Processing flow of GWX-70 radar measurements

Processing Unit (GPU)-based implementation is being investigated.

6. EXAMPLE PROCESSING RESULTS

6.1 Example 2D Results

Figure 7-8 shows example of processing results from a forward-looking scan acquired on May 30, 2013, with precipitations presenting within the 7 km range. At near range, there are two significant hard targets. One is the water tower discussed in Figure 5, the other is a building complex (Figure 7) with two separated buildings, The original MF scan output is shown in Figure 7. Figure 8(a) shows the image after the range processing, and Figure 8(b) shows the image after the cross-range processing. It is difficult to obtain detailed comparison at these spatial scales, while we can clearly see the change of resolutions. A better comparison is zooming into a smaller scale and focusing on near-range responses. These are shown in Figure 9.

In Figure 9, we compare MF outputs, range-processing-only, cross-range-processing only, as well as a 2D processing result for this scan, Images from all the four cases are zoomed to the same spatial scale and color scale. In Figure 9(a), we can see that the MF output has fairly good SNR, but the resolution is low especially for the azimuth direction. The signature of the water tower occupies multiple cells and there are significant sidelobes around them. The building complex is shown as one "blurred mass". After range processing, the range resolution shows clear improvement as well as sidelobe level, the signature of the building starts to "detach" from the blind-zone ring as a result of sidelobe mitigation, as shown in Figure 9(b).

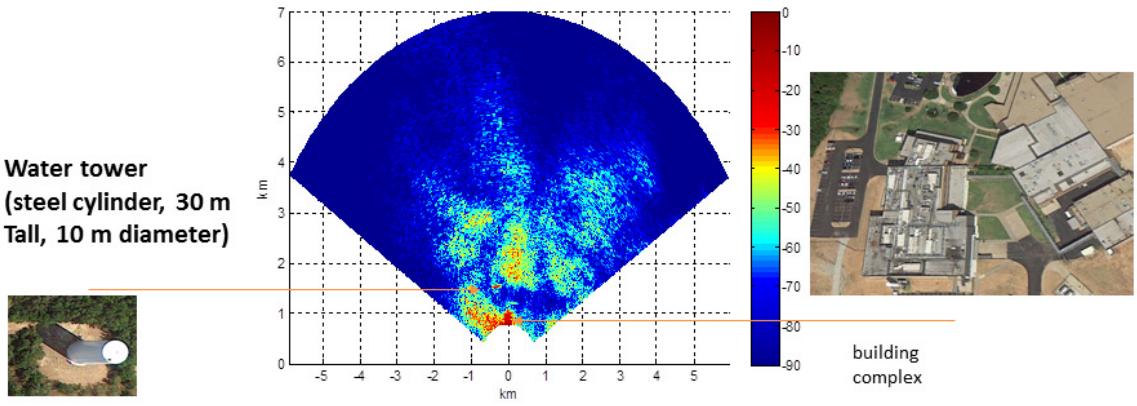

Figure 7: Sample pulse compression- PPI scan from GWX radar with observation scene description

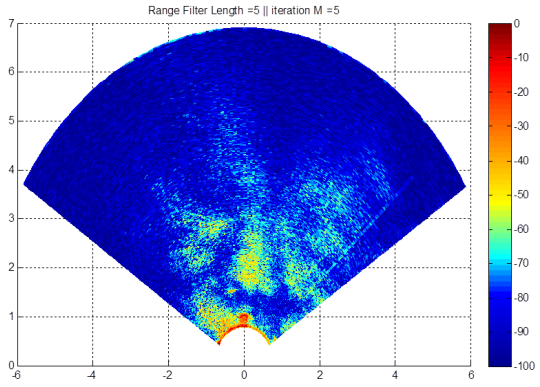

(a)

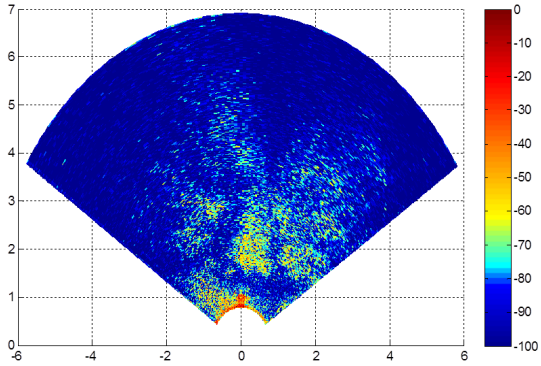

(b)

Figure 8: 2D processing procedure and example results from a single scan (averaged by 8 pulses): (a) After range processing, range filter length =5, (b) After azimuth processing, cross-range filter length =5.

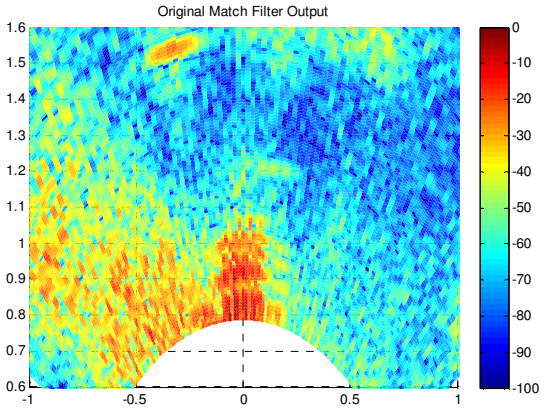

(a)

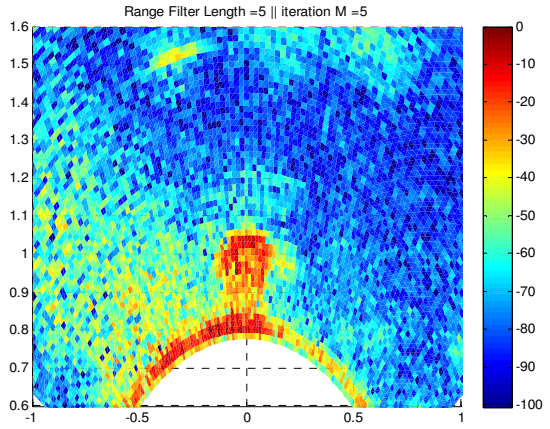

(b)

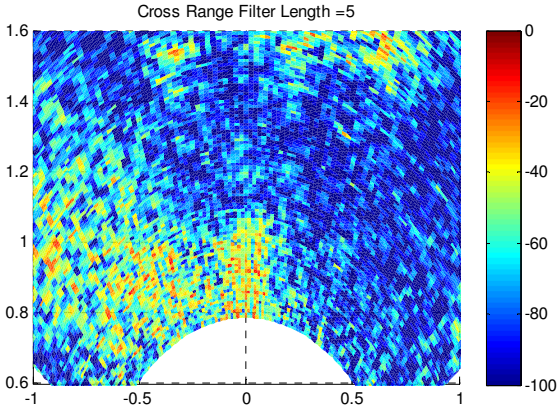

(c)

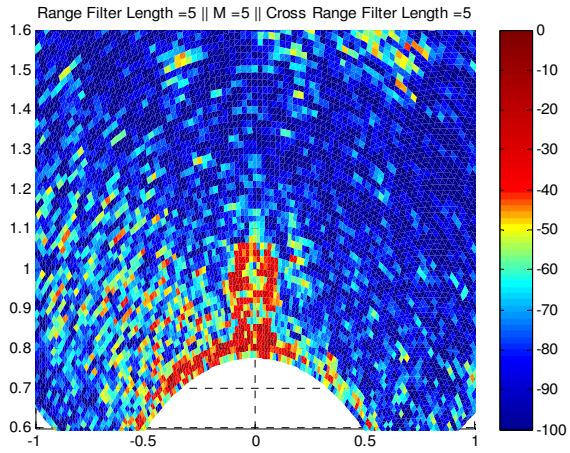

(d)

Figure 9: "Zooming-in" observation of Figure 8, (a) MF output, (b) After range processing, (c) Only azimuth processing, (d) After both range and azimuth processing.

Similarly, significant azimuth resolution improvement can be seen from Figure 9(c) in which only the cross-range processing is applied, and the two buildings start to 'separate". Lastly, after 2D processing, the water tower is basically shrinked into one resolution cell, and the two buildings are now clearly distinguishable.

6.2 Example 1D Results

We may further zoom in the 2D image and focus on the individual 1D profiles. In Figure 10, range and azimuth 1D profiles containing the water tower are plotted. Clearer observations of resolution/sidelobe/SNR improvements can be made.

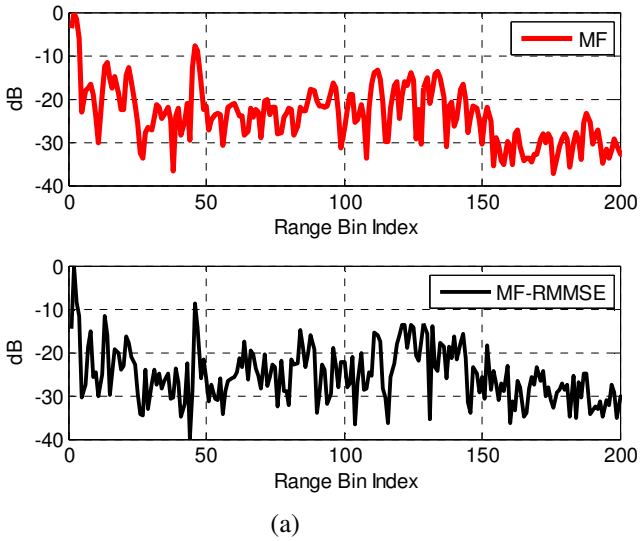

(a)

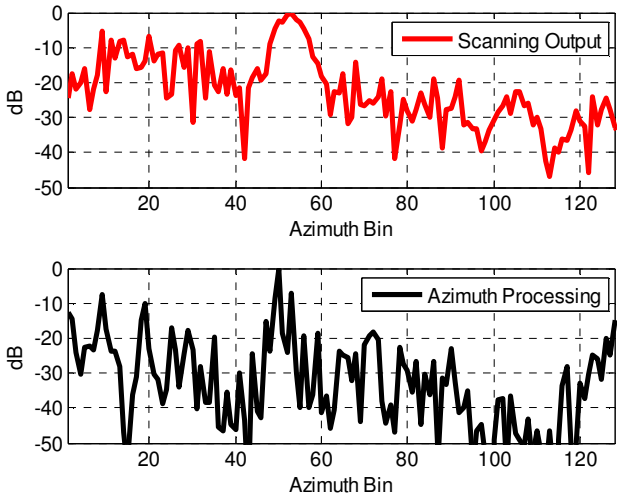

(b)

Figure 10: 1D processed profiles comparing to MF output, (a) Range profile across the water tower (located close to range bin #50, fixed azimuth = -12 degree), (b) cross-range profile across the water tower (located to cross-range bin# 50, fixed range bin index = 92).

7. DISCUSSIONS

Results so far have demonstrated improved range resolution (16m without downsanmpling, 75 m with downsanmpling), azimuth resolution (improved from 5 degree to 1 degree), and improvement of sidelobe suppression on GWX-70 radar. Performance of sidelobe suppression is a little more difficult to evaluate, as in the 2D processing, very low learning step sizes are used to compromise the "smoothness" of weather response, so the sidelobe suppressions are less aggressive than in Figure 5. However, optimal parameters can be exercised for different types of targets or scenarios, which will be further studied. More work will be performed to further reduce the computational loads by applying direct 2D processing and advanced onboard processors, as well as theoretical comparisons of different algorithms. Further developments based on these results to demonstrate realistic H-SAA missions are also planned.

8. ACKNOWLEDGEMENT

This work is a joint effort between University of Oklahoma and Garmin International Inc. Algorithm developments have been partially supported by NASA GSFC through the grant NNX11AM10A. This work also received important help from the Advanced Radar Research Center (ARRC) at the University of Oklahoma and members from the National Severe Storm Laboratory (NSSL), National Oceanic and Atmospheric Administration (NOAA).

9. REFERENCES

ASTM Standard F2411, 2007: Standard Specification for Design and Performance of an Airborne Sense-and-Avoid System, ASTM International, West Conshohocken, PA, 2007.http://enterprise.astm.org/filtrexx40.cgi?+REDLINE_PAGES/F2411.htm

Garmin International, Inc., 2013: https://buy.garmin.com/en-US/US/oem/sensors-and-boards/gwx-70/prod127591.html

Garmin International, Inc., 2013: http://garmin.blogs.com/ukpr/2012/07/garmin-brings-affordable-doppler-capable-weather-radar-capabilities-to-general-aviation-with-gwx-70.html#.Ug5bjmso5dg

Griffith, J.D., and Lee S.J., 2011: Environmental modeling for sense and avoid sensor safety assessment, 30th IEEE/AIAA Digital Avionics Systems Conference, Oct 2011.

Angelov, P. 2012: Sense and Avoid in UAS, John Wiley & Sons, 2012.

Shang. W., Li. Z., Zhang Y., 2012: "Application of Optimized Filters to Two-Dimensional Sidelobe Mitigation in Meteorological Radar Sensing", IEEE Geoscience and Remote Sensing Letters, Vol.9, pp. 778-782, 2012.